We are IntechOpen,
the world's leading publisher of
Open Access books
Built by scientists, for scientists

6,900
Open access books available

185,000
International authors and editors

200M
Downloads

154
Countries delivered to

Our authors are among the

TOP 1%
most cited scientists

12.2%
Contributors from top 500 universities

CLARIVATE ANALYTICS

BOOK CITATION INDEX

INDEXED

WEB OF SCIENCE™

Selection of our books indexed in the Book Citation Index
in Web of Science™ Core Collection (BKCI)

Interested in publishing with us?
Contact book.department@intechopen.com

Foam Materials Made from Carbon Nanotubes

Kyuya Nakagawa
Research Centre for Nano-Micro Structure
Science and Engineering,
University of Hyogo,
Japan

1. Introduction

1.1 What is CNT foam?

Foam is a macroporous material and comes in many forms, such as polystyrene shock absorbers, dish-washing sponges, and foam board insulation. This chapter describes a technique to prepare foam materials from carbon nanotubes (CNTs). The use of a CNT-made foam as a kitchen sponge may not be a good idea, however. We of course expect the nano-carbons to have a specific functionality on the prepared bulk material. A challenge would be to place a function derived from nanomaterials on a bulk structuralized material. It would be highly useful to make up a material with a specific function that is attained only by nano- and micro-structuralization. A major feature of a foam material is that it has a function derived from its microstructures (macropores). The present chapter discusses a preparation strategy to produce a material with controlled microstructures from CNTs.
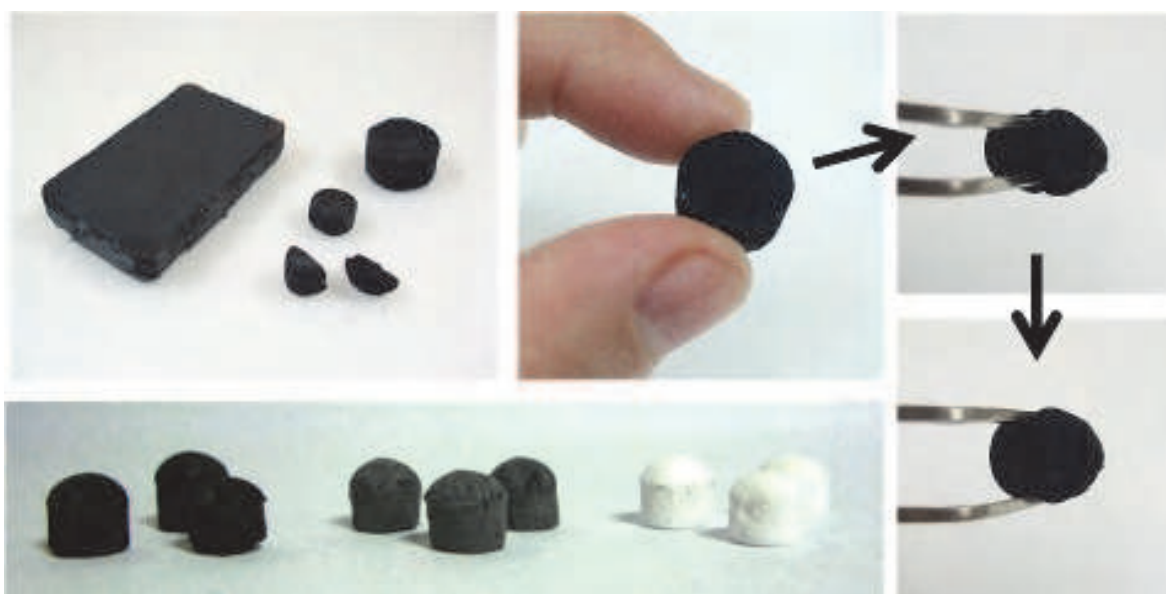

Fig. 1. Foam materials made from carbon nanotubes. Samples in grey and white (pictured bottom left) were prepared by mixing titanium nano-powders.

1.2 How is it made?

Recent studies explain how to make from CNTs highly porous foam materials, which are composite materials made from polymers and CNTs. CNT foams can be prepared using several methods, as illustrated in Fig. 2. One is a bottom-up method using phase separations induced by thermal phase transition, polymerization reaction, solubility shift, and so on. When a phase separation is induced in a CNT suspension, a phase that cannot include dispersed materials (such as CNTs) generates a counter phase in which the dispersed materials are concentrated (concentrated phase). Frequent phase separation produces a microstructure in the resultant solution after the pure phases are removed by post-treatment. As shown in Fig. 2A, this phase separation route is mainly realized by a gas-liquid phase separation process (foaming) and solid-liquid phase separation process (freezing). CNT foam preparation using a poly(vinyl alcohol) foaming process was first reported by Shaffer and Windle (1999). Subsequent researchers found that foaming processes with polystyrene, polyurethane, poly(methyl methacrylate), and so on showed potential in preparing CNT foam with controlled pore structures (Shen et al., 2005; Park & Kim, 2008; Xiang et al., 2009; Chen et al., 2010; Hermant et al., 2009; Zeng et al., 2010).

It has long been known that freeze-drying a solution results in porous materials, where the pore structures are replicas of the ice crystals formed during freezing. However, it was only recently that an attempt was made to prepare porous CNT foams via freeze-drying. Nabeta and Sano (2005) conducted a trial to prepare freeze-dried CNT foams from a CNT-gelatin aqueous suspension. This would make it the first study to employ a solid-liquid phase separation process for producing macroporous CNT foams (in their report, they stated that the microstructures were created by gelatin gel formation; however, this may be only partly true: gel formation contributes to producing nanostructures, whereas ice creates microstructures). In any case, it has clearly been shown by related studies that ice is an interesting tool for creating interconnected 3D microstructures in a freeze-dried CNT foam (Lau et al., 2008; Thongprachan et al., 2008; Kwon et al., 2009; Olivas-Armendariz et al., 2010; Nakagawa et al., 2010). Fairly well-aligned beautiful macropore formations in the freeze-dried foams have been demonstrated by a Spanish group during intensive practical studies (Gutiérrez et al., 2007a; 2007b; Abarrategi et al., 2008).

Phase separation techniques would allow further processing variations, as described in a report by Leroy et al. (2007). They demonstrated CNT foam preparation via a bubbling and subsequent freeze-drying process that enabled unique microstructure formation. Sol-gel processing would also be useful in producing CNT foams with nano-structured CNT arrays (Worsley et al., 2009). In order to create a controlled microstructure by using a phase separation process, we must control the kinetics of the phase transition (e.g. evaporation for foaming process, solidification for freezing process). In this regard, freezing would be advantageous for planning an engineering strategy because freezing can simply be controlled by a thermal system. The following sections deal with the processing strategy for obtaining desirable microstructures on a CNT foam prepared via a phase separation process induced by freezing.

As depicted in Fig. 2B, CNT deposition onto a ready-made foam material is an alternative CNT foam preparation method (Boccaccini et al., 2007; Ji et al., 2009; Zawadzak et al., 2009; Meng et al., 2009). It is one type of coating technique for CNTs on a porous media. Pore structures of the media can be appropriately designed using a number of other methods.
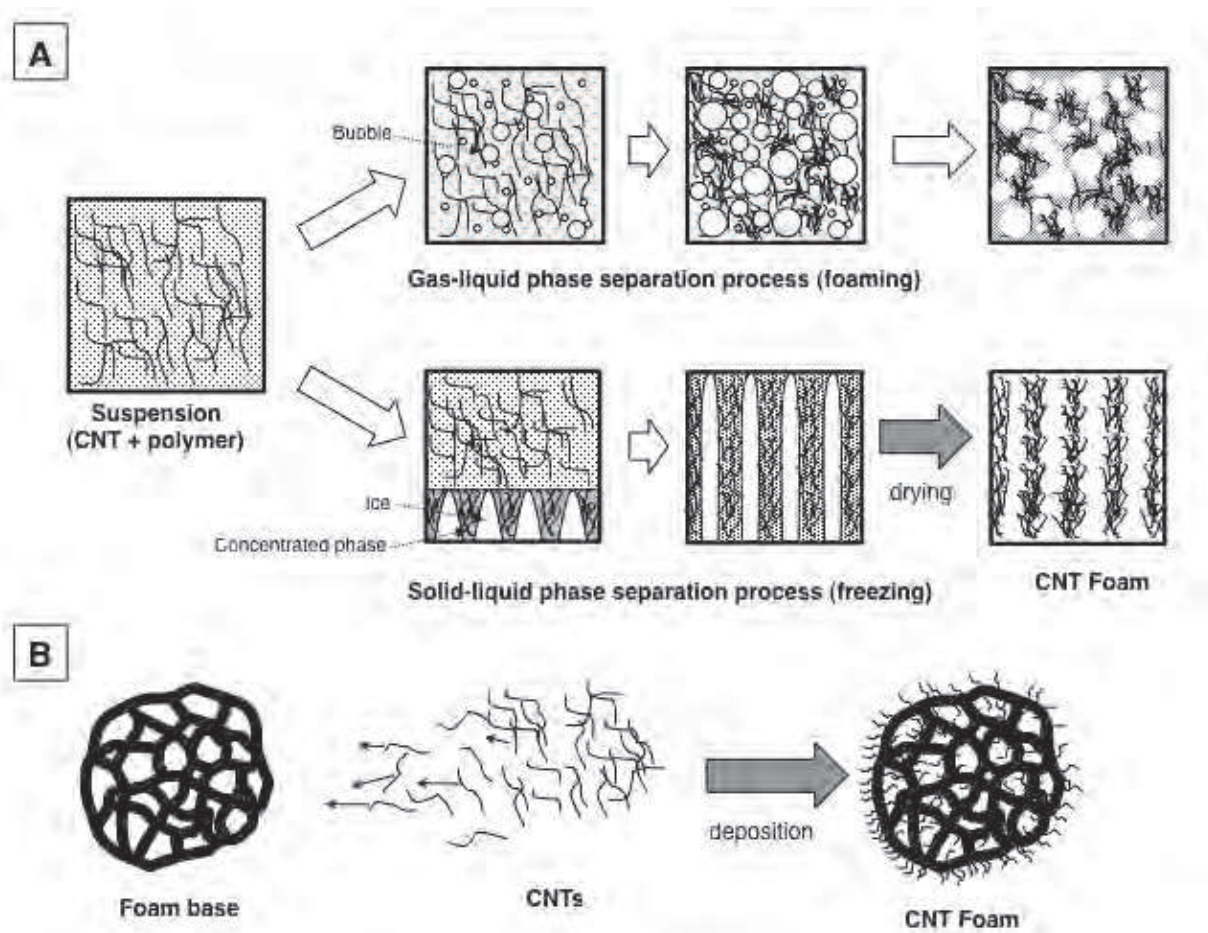
Fig. 2. Foam material preparation from carbon nanotubes.

2. Freezing as a tool to control microstructure

2.1 Solidification of colloidal suspension

Freezing induces a pattern formation in a colloidal suspension when the velocity of freezing front progress is maintained at a certain value. The microstructure of a frozen colloidal suspension cannot be obtained by simply replacing the water in unfrozen solution by ice. The freezing front rejects suspended particles when the front velocity is sufficiently low. However, it engulfs particles when the velocity is too high. The physics of this particle rejection phenomenon at the solidification front have been investigated based on several theories (Wilde & Perepezko, 2000). It has recently been identified that interfacial premelting phenomena virtually control the behaviour of a foreign particle at the solidification interface (Dash et al., 1995, 2006; Wettlaufer & Worster, 2006). When a solidification interface meets a particle, repulsive intermolecular interaction between the solid and the particle creates a thin liquid layer for reducing total free energy at the interface (reducing instability caused by the repulsive intermolecular interaction). This liquid layer formation, due to interfacial premelting, allows a particle to move away from the freezing front by repulsive interaction with the ice (Fig. 3). The repulsive force is a dominating factor that controls the particle transfer kinetics. Put simply, a particle is rejected by the ice front when the particle mass-transfer velocity is higher than the ice front velocity; otherwise it is engulfed. Following this theory, suspended particles are sometimes rejected and engulfed in a frozen bulk to form a

complex microstructure. Further theoretical approaches predict a periodicity of microstructures made by ice in a colloidal suspension (Peppin et al., 2007, 2008, 2010). However, as yet, no complete theory has yet been put forward for designing a micrometre-scale 3D architecture constructed by ice.
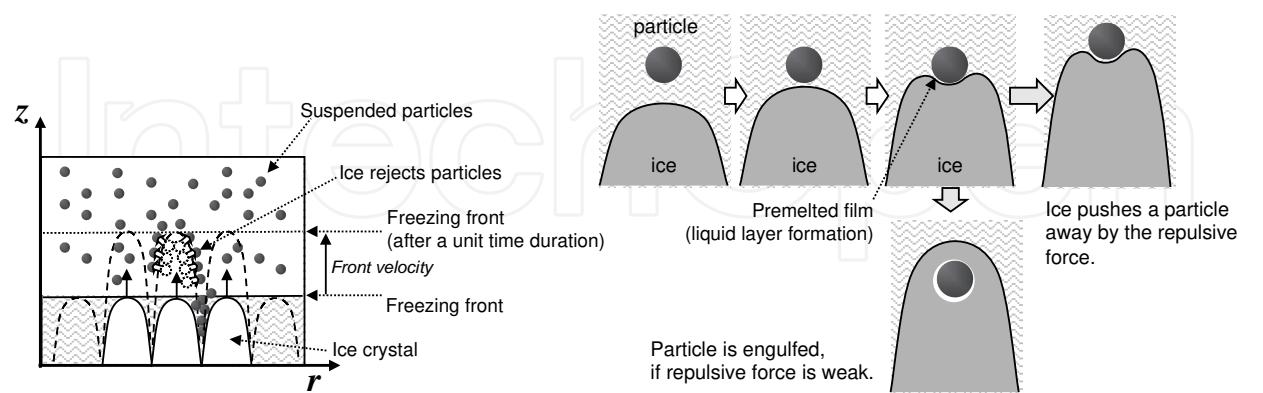

Fig. 3. Schematic illustration of the solidification of a colloidal suspension.

2.2 Engineering approach

This section describes an engineering approach to assessing microstructure formations in freeze-dried CNT foams prepared via several processing routes. As shown in Fig. 4, freezing was performed via either contact freezing with a heat exchanger or immersion freezing in a cryo-bath. Details of these experiments can be found in a report by Nakagawa et al. (2010). These two freezing methods make it possible to prepare several types of microstructures, as explained in the following.
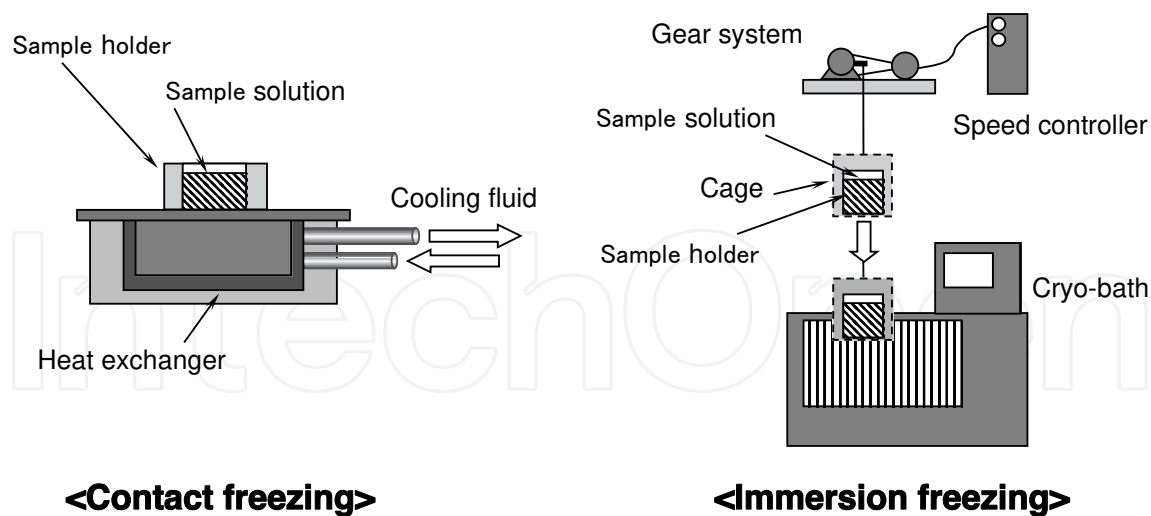

Fig. 4. Freezing methods.

2.2.1 Materials and methods

Materials

Commercial multi-walled CNTs (MWCNTs) (Bayer Materials Science Ltd., 13–16 nm mean outer diameter, 1 to >10 µm length, purity >95%, synthesized by chemical vapour

decomposition) were used in this work. Carboxymethyl cellulose (CMC) sodium salt surfactant (Fluka, Sweden) was used as a dispersing agent. Some 1 wt% of MWCNT was dispersed in 10 mL of an aqueous solution of CMC sodium salt (1 wt%) with the aid of an ultrasonic homogenizer (UH-300, SMT company, Japan) for 30 minutes at 15 W output. The suspension thus obtained was placed in a sample holder equipped with a cooling device.

Contact freezing

A 0.25-mL acrylic sample holder (diameter $D = 8$ mm, height $H = 5$ mm) was fixed on a heat exchanger, through which a liquid coolant (methanol) was continuously circulated to control the temperature of the sample. With this external arrangement, the freezing phenomena would not be affected by artificial obstacles. In the experiment, the sample solution temperature was initially stabilized at an ambient temperature (25 °C) for 15 minutes, then cooled to -40 °C at a selected cooling rate, namely -3.0 or -0.1 °C/minute. The frozen sample thus obtained was consecutively freeze-dried on the same cooling shelf. It should be noted here that the observed cooling rate was the value used by the cryostat to control its circulating coolant temperature, which may differ slightly from the temperature of the heat exchanger surface that contacted the sample solution.

Immersion freezing

An immersion system equipped with an electrical gear system was designed to lower a sample cage at a fixed speed into a cryo-bath, whose temperature was maintained at a selected value (-40 °C with methanol, or -196 °C with liquid nitrogen). A thin square copper plate was attached to the bottom edge of a glass tube (inner diameter $D = 8$ mm, height $H = 15$ mm, wall thickness $d = 1$ mm), and the setup was placed in a cage. The glass tube was filled with the sample solution and left to equilibrate to room temperature. It was then arranged in the immersion system in such a manner that the sample bottom lay just above the pre-cooled coolant surface. The cage was lowered into the cryo-bath at a selected immersion speed (67 or 20 µm/s) until the coolant level almost reached the top edge of the sample tube. The obtained frozen sample was then immediately transferred from the cage to the cooling shelf of the freeze-dryer.

Freeze-drying

The frozen sample was placed on the shelf of a heat exchanger pre-cooled at -40 °C. After evacuating the system (chamber absolute pressure of 10–20 Pa), the shelf temperature was reset at -20 °C, and the samples were left under these conditions for four days to complete the sublimation. The drying curves of various CNT solid foams have been reported in previous work (Nakagawa et al., 2008). Typically, it took approximately 60 hours to finish the drying process under the chamber pressure of 10 Pa and shelf temperature of -20 °C.

Model calculation

Temperature profiles during the freezing steps were simulated via a mathematical freezing model developed by Nakagawa et al. (2007) in order to estimate freezing front geometry, freezing front velocity, and temperature gradient in a frozen zone. The mathematic model was based on classical Fourier-type thermal conduction equations and solved by commercial finite-element analysis software, COMSOL 3.6. The 2D axisymmetric model took into account the real geometry of the sample container and its surroundings, drawn using the software. The key details of this modelling approach (e.g. basic equations, model

geometry, boundary conditions) are explained in previous publications (Nakagawa et al., 2007, 2010).

2.2.2 Microstructures of the prepared foams made from CNTs

A foam material possesses porous microstructures, as noted in the Introduction. The microstructure of the prepared CNT foam were observed with SEM, as depicted in Fig. 5. These images confirm that fine macropores were formed with a particular regularity. A typical microstructure obtained via contact freezing was a bundle of cylindrical pores (Fig. 5a). A layered monolith was prepared via immersion freezing (Fig. 5b). By enlarging the matrix of the pore wall, it was found that it was made from CNTs. However, it must be borne in mind that these architectures are maintained by the polymers that help CNTs to disperse in the original solution. The sponge-like elastic feature of a typical CNT foam sample could be clearly observed via this polymer (Fig. 1). The foam materials prepared in the presented methods were highly porous, with a porosity of about 95–98% and a bulk density of 0.05–0.06 g/cm^3.
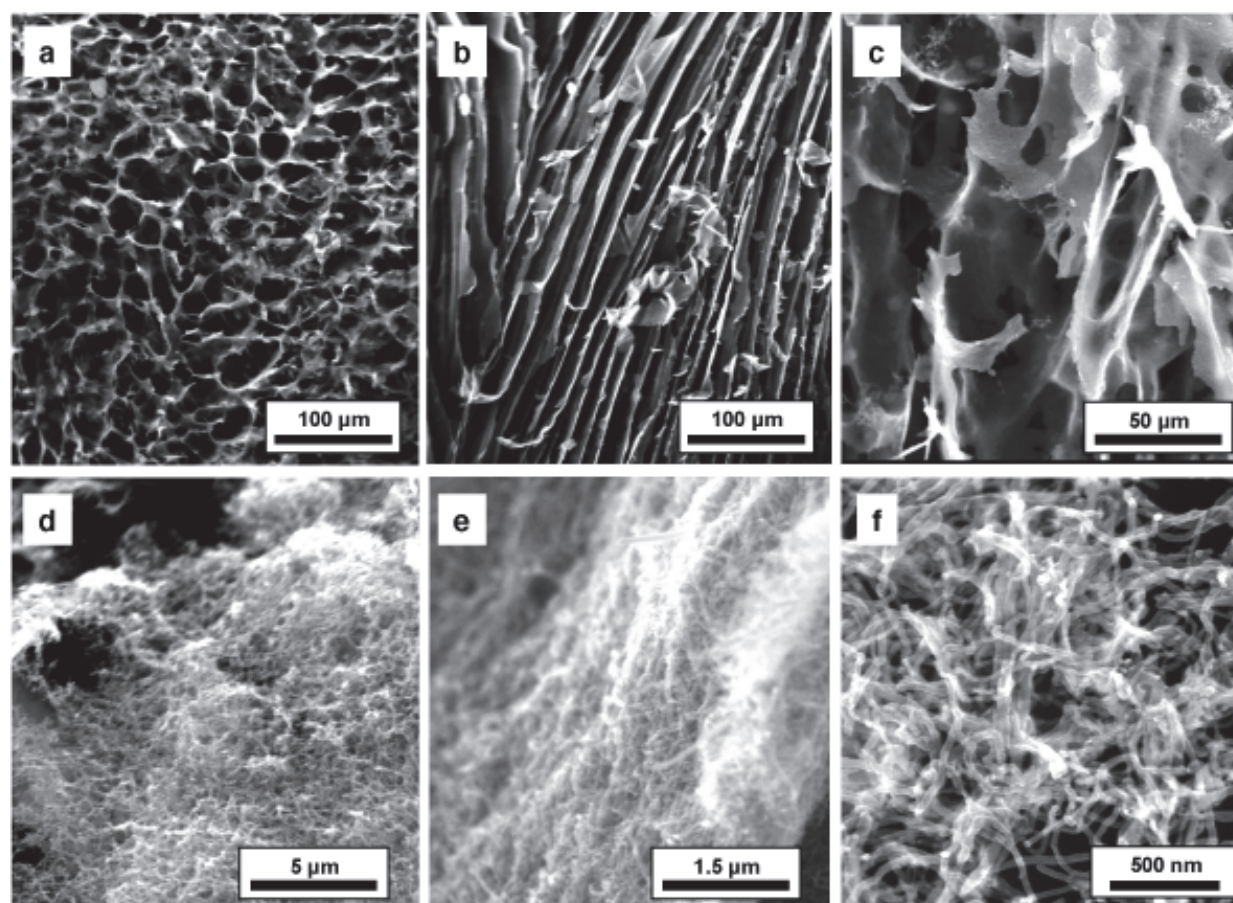

Fig. 5. SEM images of CNT foams: (a) a sample prepared via contact freezing, (b) a sample prepared via immersion freezing, (c)–(f) foam matrix images taken at various magnifications.

Microscopic images of the prepared CNT foams are shown in Fig. 6. The black domain consists of the CNTs, and the brighter portions represent the pores of the freeze-dried samples. The 2D images were obtained after embedding the samples in epoxy resin. First, it

is evident that the domain of the CNTs exhibits a fairly well-interconnected network. It is also clear from these figures that the observed pore sizes were influenced by the freezing condition, while the microstructures were dependent on the freezing method. Comparison of the horizontal and the corresponding vertical cross-sectional images of a sample prepared via contact freezing at a fast cooling rate reveals that both were assembled of mostly columnar pores (Fig. 6A-1, -2). In fact, it is difficult to find clear differences or tendencies in their morphology, which suggests that the growth directions of ice crystals along the z and r axes were quite random. In contrast, lamellar structures were observed on the horizontal cross-sectional images obtained via a slow cooling rate ((Fig. 6B-1) while columnar structures appeared on the vertical cross-sections (Fig. 6B-2). This fascinating contrast suggests that ice crystal growth along the z-direction was constrained by the slow cooling condition. The cooling rate was a key parameter that decided the mean pore size, if the sample was frozen with a contact cooling plate. In short, a faster cooling rate led to smaller macropores. Generally, smaller pores appeared at the bottom of the sample. This is because the ice crystal growth rate was extremely rapid just after the breakpoint of supercooling. After the onset of supercooling, ice crystals grew at a moderate velocity controlled by the thermal flux through the system, thereby resulting in larger pore sizes.

Interestingly, when samples were frozen via immersion freezing, we could observe an obvious morphological difference. Continuous lamellar structures commonly appeared on the vertical cross-sectional images (Fig. 6C-2, 6D-2), and columnar structures appeared on the horizontal cross-sectional images although their aspect ratio was sometimes very large (Fig. 6C-1, 6D-1). Ice crystals predominantly grew in the z-direction, and bundles of uniformly arranged dendritic ice crystals contributed to construct a honeycomb monolith. Even though slightly smaller pore sizes were observed at the bottom of the sample owing to the influence of a supercooled layer, the lamellar structures along the z-direction appeared rather uniformly throughout the entire sample height. In fact, the immersion rate influenced the aspect ratio of the columnar cross section. In short, the aspect ratio became larger when the samples were immersed more slowly, suggesting that the aspect ratio depends on a kinetic balance between the ice crystal growth rates along the z- and r-directions.

As previously explained, the ice crystal growth rate was found to correspond roughly to the immersion rate, although the mean pore size did not show a linear relation to the latter. Incidentally, it is worth noting that, although the mean freezing front velocity of sample A1, which was experimentally detected as ~25 µm/s, was essentially equivalent to the immersion rate of B3 (20 µm/s), the microstructures of these two samples are by no means similar. In other words, it is necessary to discuss how these microstructures were produced based on rational data that essentially govern ice crystal appearance and growth during the freezing stages.

2.2.3 How does freezing control microstructure?

A model calculation is a useful tool to estimate property data taking into account the geometry of the sample undergoing a transient process. The freezing process is a transient process that is controlled by thermal flux in a sample solution. The phase transition of water (solidification) provides latent heat to the system. Therefore, the heat must be removed from the system for the continuance of freezing. Thermal flux strongly relates to sample geometry, the thermal conductivity of each component (e.g. solution, solid layer, sample holder, ambience), and cooling protocols. A mathematical model has been developed by the
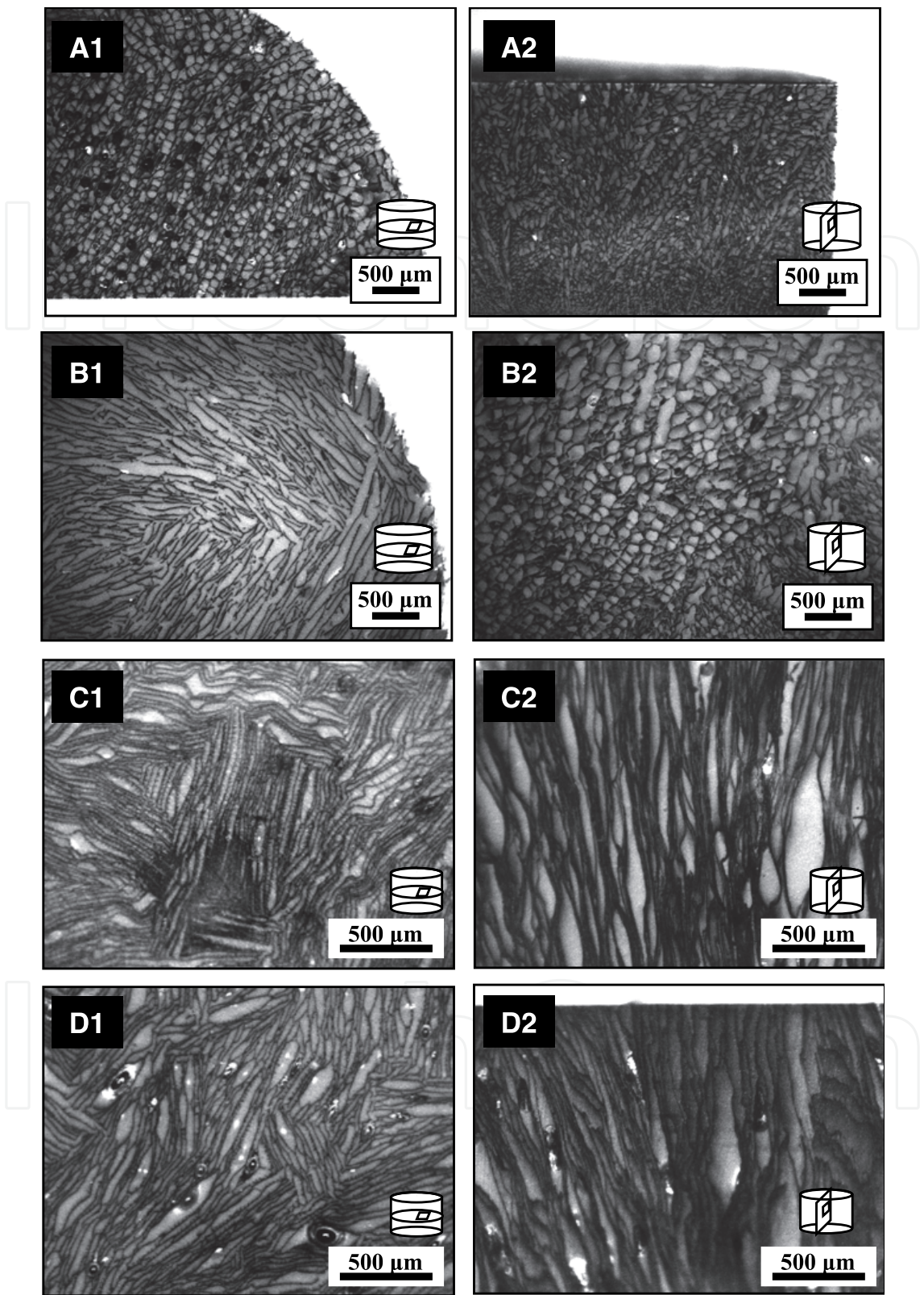
Fig. 6. Microscopic images of CNT foams: (A1, 2) sample prepared via contact freezing (−3 °C/min), (B1, 2) sample prepared via contact freezing (−0.1 °C/min), (C1, 2) sample prepared via immersion freezing (67 μm/s), (D1, 2) sample prepared via immersion freezing (20 μm/s).

author, as reported in previous publications (Nakagawa et al., 2007, 2010). By using the mathematical model simulation, we can obtain thermal histories of the sample solutions during contact freezing and immersion freezing. These thermal profiles are useful for predicting microstructure formation in a freeze-dried foam material.
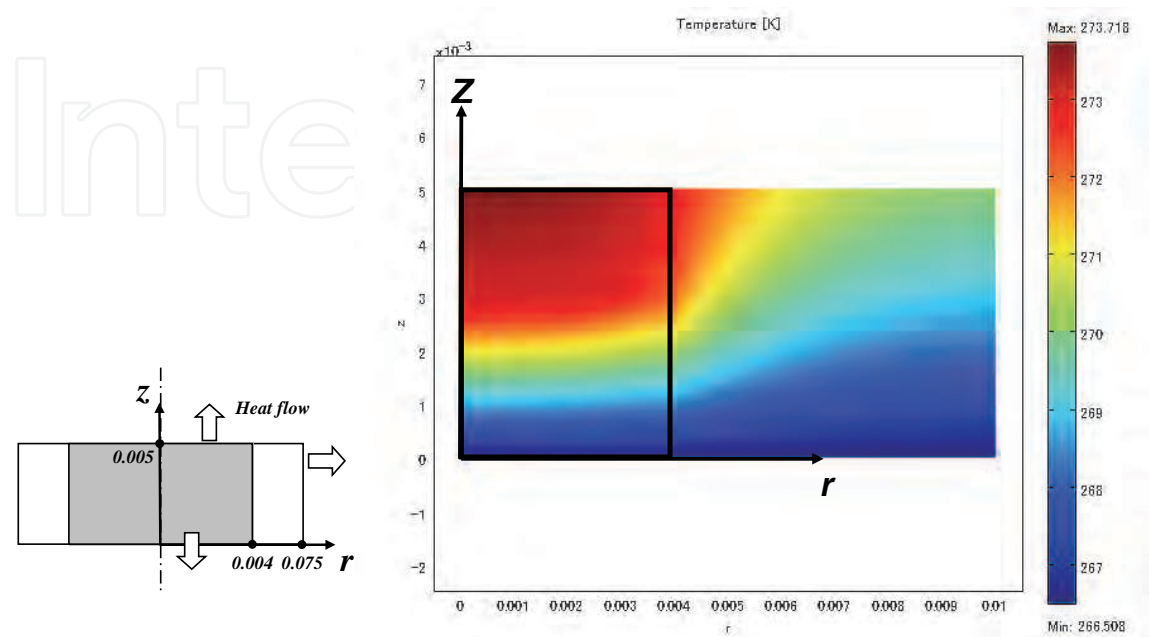

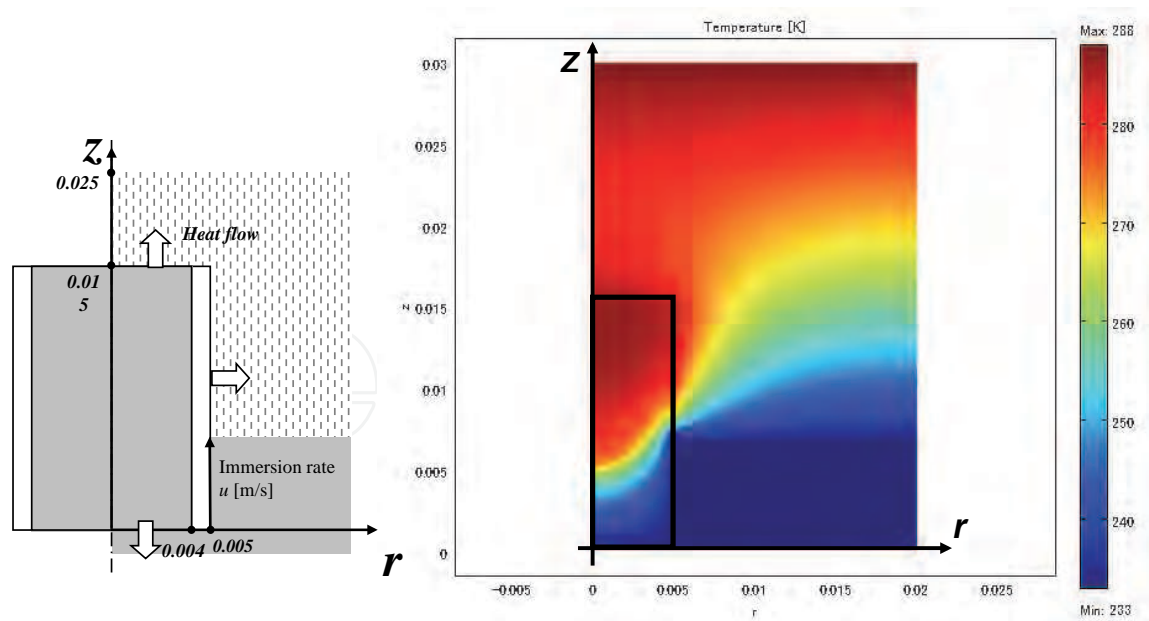Fig. 7. Temperature profile during freezing (contact freezing).

Fig. 8. Temperature profile during freezing (immersion freezing).

Through microscopic observation it was found that the present two freezing protocols lead to unique microstructures. The most fascinating feature of the immersion freezing is the appearance of a uniformly arranged monolithic layered microstructure in the sample, which was not observed in the samples prepared via contact freezing. Both freezing methods can

be referred to as unidirectional freezing systems. However, even if the freezing rates were adjusted to achieve equivalent values for both contact and immersion freezing, we cannot produce samples with equivalent microstructures. This suggests that the ice formation must be identified by the geometry of the system. The term "unidirectional freezing" risks misidentification of a freezing system if it is used without identifying the thermal flow in the freezing system. Figures 7 and 8 are snapshots of the thermal profiles during contact freezing and immersion freezing, respectively. For both types of freezing, the freezing fronts move on vector $(r, z) = (0, 1)$, so that we may call this "unidirectional freezing". However, the shapes of the freezing fronts differ greatly from one another. We can confirm the differences more clearly with the concrete calculated values in Fig. 9. It is strongly believed that this is a critical parameter that determines the 3D microstructure made by ice.

Let us focus on the overall growth direction of the growing ice crystals in a newly appearing freezing layer (thickness R, in unit time), as sketched in Fig. 10 and Fig. 11.
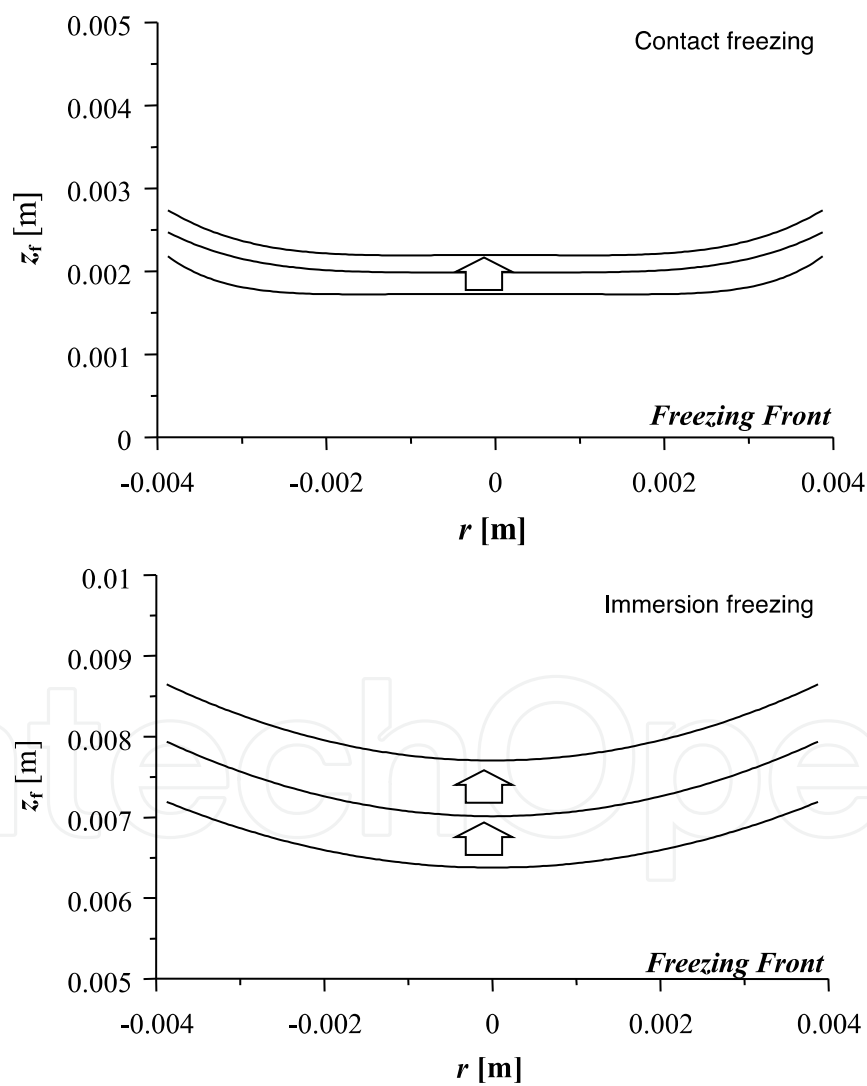
Fig. 9. Freezing front geometries.

If a freezing front is flat as simulated during contact freezing, the temperature distribution in the layer would allow a growing ice crystal to choose an arbitrary growth direction on the

interface unless there is some obstructing ice. In addition, the typical microstructures obtained via contact freezing were randomly assembled columnar ice crystals (Fig. 6-A), while the lamellar structures only appeared in the samples prepared at a slower cooling rate (Fig. 6-B). Specifically, the relatively slow freezing front velocity (small R values) mean that ice crystal growth was permitted only in a layer of limited thickness per unit of time (Fig. 10), thereby resulting in the rather unique microstructure shown in Fig. 6-B.

When we employ immersion freezing, we should bear in mind that the freezing front is curved, as shown in Fig. 9. In this case, several scenarios may lead to the creation of the unique microstructure observed in the samples (Fig. 6-C, D). First, an existing ice crystal at an adjacent higher freezing front level would present a barrier for the growing ice crystal, and as a consequence, there would be less opportunity for growth in the +r-direction. In the second scenario, no ice crystals can grow into a domain where the temperature is higher than the equilibrium freezing point. By this reasoning, the zone in which ice grows toward the –r-direction in unit time is controlled by the vector **R** (Fig. 11). Therefore, it may be that isotropic ice crystal growth (toward the z-direction) is encouraged during immersion freezing, while anisotropic growth is permitted under contact freezing. The temperature gradient in an already frozen zone should influence the choice of the direction because a larger temperature gradient would encourage z-direction crystal growth whereas a smaller gradient would lead to tilted ice growth (Deville et al., 2007). The simulation results predict that the temperature gradient values during immersion freezing are larger than their contact-freezing counterparts. However, this is not a parameter that exclusively governs the isotropy of ice crystal growth.

These insights suggest that, although the basic ice crystallization phenomena (and subsequent particle rejection phenomena) were comparable in both freezing methods, the observed temperature distribution and the movement of the freezing front in the entire freezing bulk essentially controlled the ice crystal morphology in the frozen matrix. Thus, a practical design of material microstructures for the freeze-drying process could be achieved via controlling thermal flow through the freezing system.
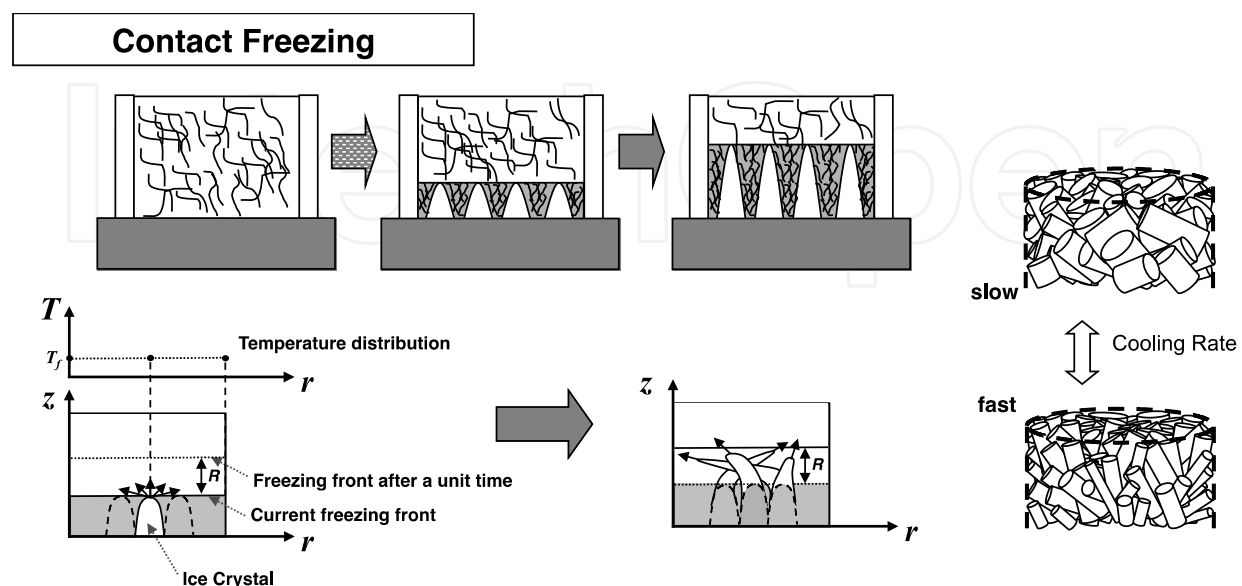

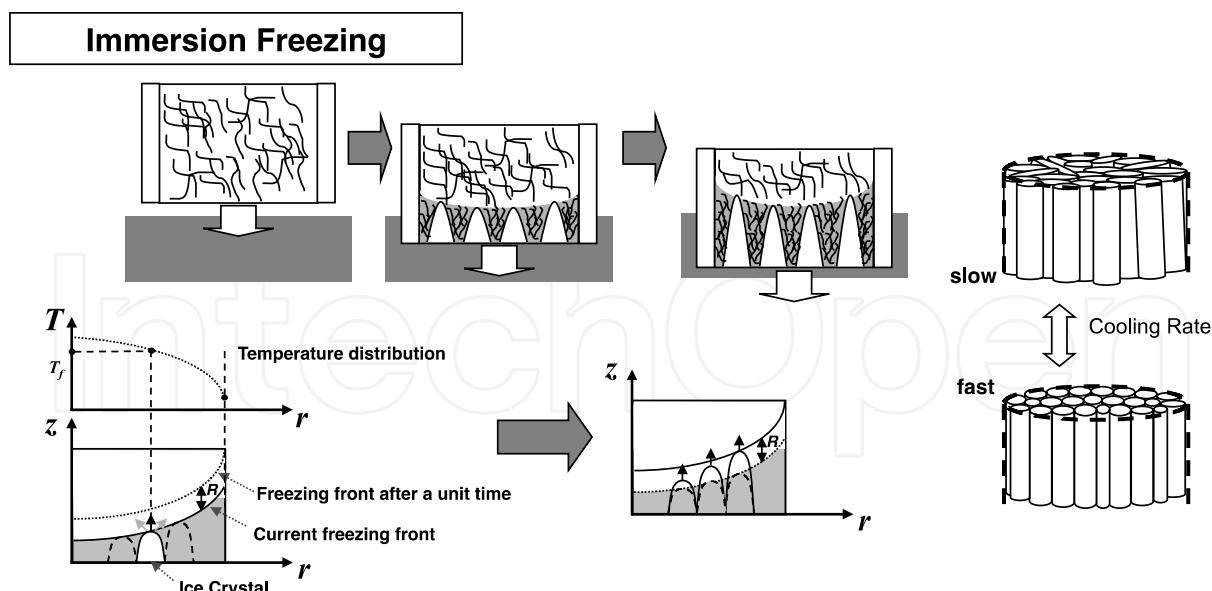Fig. 10. Sketches of ice formation during contact freezing.

Fig. 11. Sketches of ice formation during immersion freezing.

3. Insights into the functional properties

3.1 A bulk material derived from nanomaterials

As is widely known, some nanomaterials have specific functions that are primarily evoked at the nanometre scale, so that much research has been carried out for the nano-tech industries. CNTs are one of the most intensively studied nanomaterials. However, no promising commercial application based on CNTs has yet been found. CNT foam is a material with a porous structure (microstructure) constructed with nano-porous carbon, that is, CNTs. It would be reasonable to expect that CNT foam attains functions derived from both its nanostructure and its microstructure. As discussed above, we can produce CNT foam whose microstructure is controlled with a particular regularity. The following sections describe several attempts that corroborate the characteristics of CNT foams derived from CNTs and their microstructures.

3.2 Electrical conductivities of CNT foams
3.2.1 Response to the ambient pressure

In this section, we discuss the electrical conductivity of the prepared CNT foams. The foam samples prepared in this work showed electrical resistivity in the range of 1–10 $k\Omega/m$. This is of course derived from interconnected CNTs in a foam material. It is known that the CNT is an excellent adsorbent for gas molecules owing to its huge surface-to-volume ratio, hollow geometry, and unique electrical properties (Sun et al., 2007; Chang et al., 2008). In addition, a detectable change in electrical conductivity of the CNT is connected to the process of gas adsorption–desorption on the nanotube surface (Romanenko et al., 2007). Electron transfer through the CNTs is promoted when certain gas molecules are adsorbed onto the CNT walls (Chang et al., 2008). In other words, the electrical conductivity of the CNT is dependent on the interactions between the adsorbed gas molecules and the CNT wall. Similarly, it has been reported that the electrical resistance of the CNTs respond sensitively to the adsorption of various gases (Suehiro et al., 2003; Quang et al., 2006). In this sense, the CNT has recently become a good candidate

as a sensitive material for the detection of gases such as H_2, O_2, NO_x, NH_3, and VOCs with improved real-time monitoring (Sayago et al., 2008). It would therefore be reasonable to expect these features in CNT foams and to anticipate a link between the gas detection feature and microstructure of CNT foam.

We connected probes to the prepared CNT foam with conductive adhesive. The sample with the probes was placed in a vacuum chamber, and the pressure in the chamber and electrical resistivity were monitored with a digital multimeter. Figure 12 shows typical examples of the relationship between the electrical resistivity of the CNT foam and the chamber pressure. It is clear that the resistivity responds rapidly to the rise and drop in the pressure. It is straightforward to attribute this change in electrical resistivity to the adsorption and desorption of air on the foam walls composed of CNTs. It was found by the author's research group that the absolute resistivity value decreased with increasing CNT content, and the specific value of resistivity difference (corresponding to 0.1 MPa pressure difference) decreased with increasing CNT content (Thongprachan et al., 2008). The contacts between the CNTs in the bulk walls were influenced by the CNT concentration, and the difference in the contacts appeared as a difference in the electrical resistance of the sample.

What would happen if we introduce a gas other than air into the evacuated chamber? Attempts were carried out with He, ethane, and iso-butane. These three inert gases differ in molecular size. We expected that the microstructure formation in CNT foam may influence the diffusivity of these gases. Samples prepared via contact freezing and immersion freezing were employed for this dynamic electrical response test, with the results shown in Fig. 13.
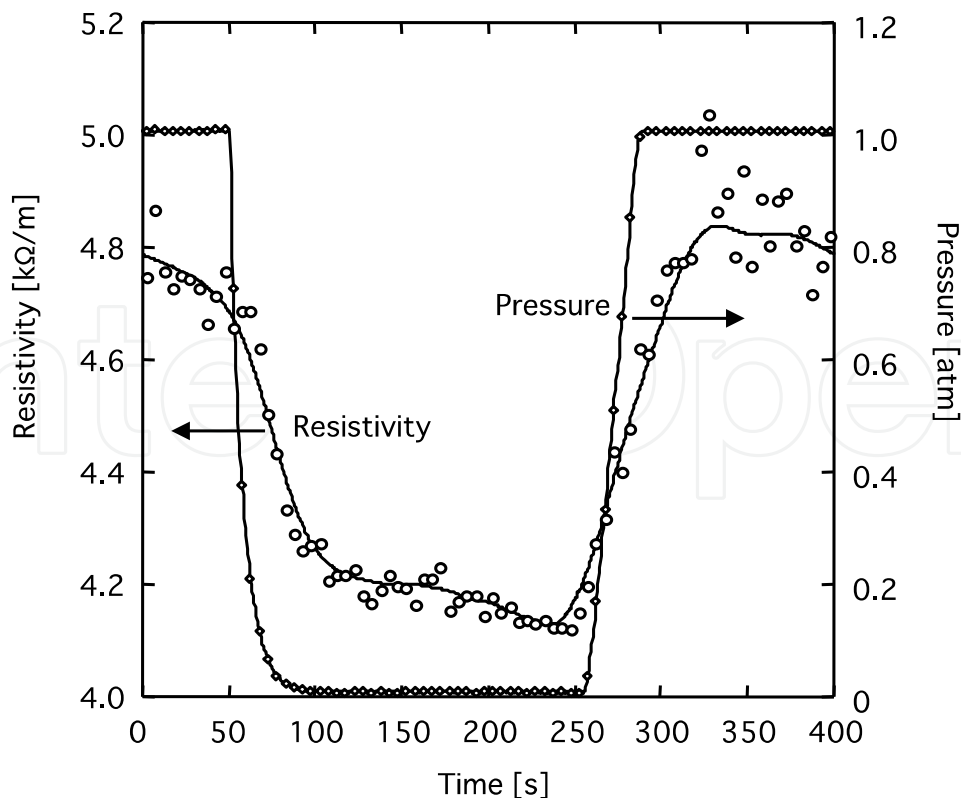

Fig. 12. Relationship between electrical resistivity and gas pressure for CNT foam.
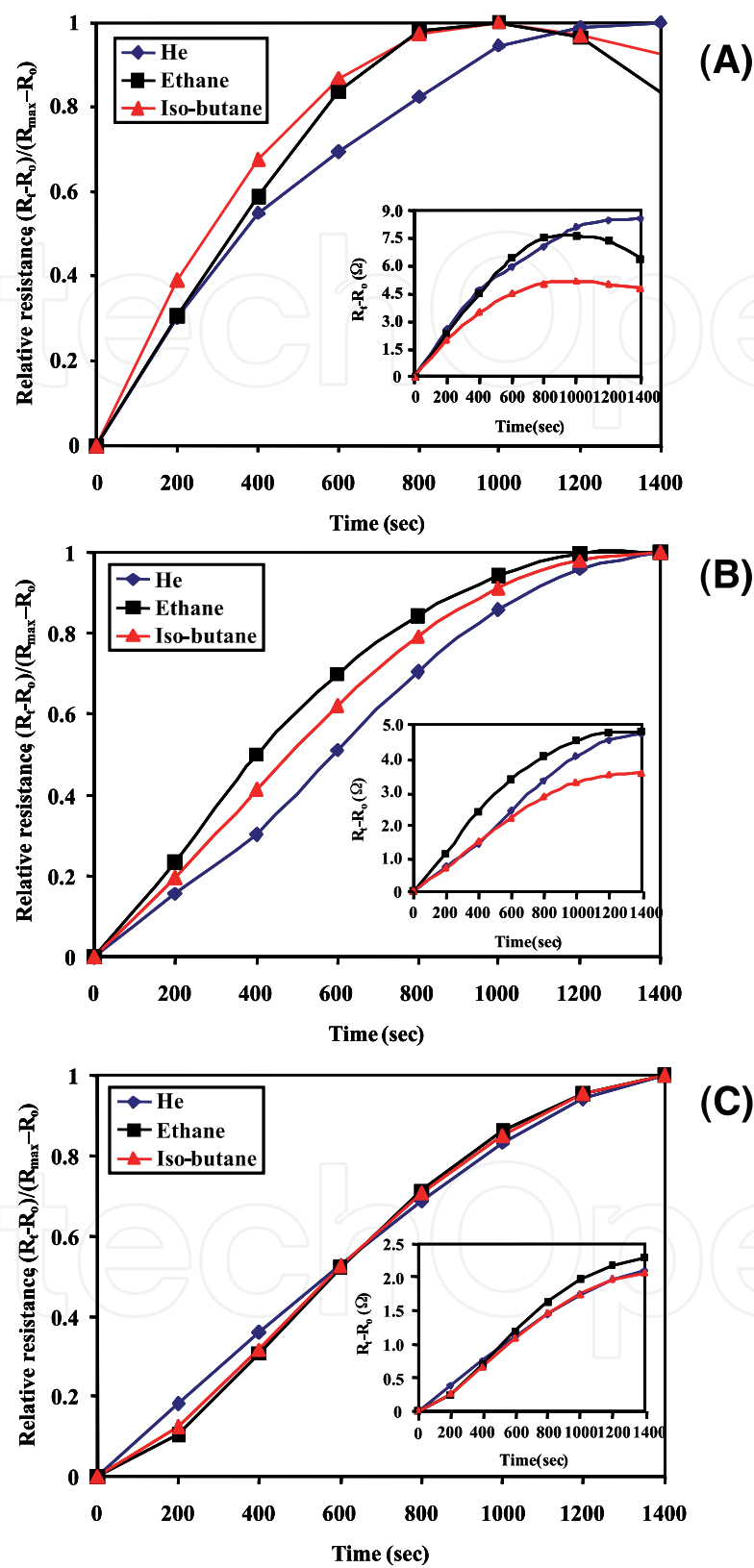
Fig. 13. Dynamic electrical response of CNT foams against uptake time for He, ethane, and iso-butane. Sample prepared: (A) via contact freezing (slow cooling), (B) via contact freezing (rapid cooling), and (C) via immersion freezing.

As expected, the gas type and microstructure appear to be related to the electrically conductive characteristics of the CNT foams. It was clear that different patterns of normalized gas-uptake electrical response appeared for each CNT foam specimen after coming into contact with each of the three test gases. The pattern difference corresponds to a difference in the freezing conditions. As described in the previous section, the CNT foams produced via contact freezing possessed a pore structure with randomly oriented columnar pores, whereas the immersion freezing method gave uniformly oriented pore structures. The freezing conditions (i.e. cooling rate or immersion rate) significantly affected the pore size. In short, CNT foam produced with a faster freezing rate usually had a smaller macropore size. For the sample prepared via contact freezing, among the three tested gases, it was found that He attained an equilibrium state most slowly (Fig. 13-A). In fact, the required gas adsorption equilibrium time increased approximately in the following order: iso-butane = ethane < He. Surprisingly, no significant differences in the normalized responses were observed between the three gases in the case of CNT foam obtained via immersion freezing.

It may be logical to attribute the resulting differences in the normalized gas-uptake electrical response for each gas species to the gas diffusion process in CNT foam. It was ensured that each CNT foam specimen used in this experiment possessed significantly different microstructures. The macropores, however, are not sufficiently important in controlling the mass transfer of gases such as He (they consist of almost free space in terms of angstrom-scale molecules). Therefore, it would be reasonable to conclude that the nano-space made by CNT assembly is the major factor in controlling gas diffusion regimes, and that the manner of ice formation controls the nanostructures made by CNT arrays. Direct evidence for shedding light on whether ice creates such a structure is still lacking. However, this may be possible because ice pushes CNTs away in creating a microstructure during freezing. Considering the repulsive force balance between ice and a suspended tubular-shaped nanomaterial (CNT), a directional force provided by an ice crystal would allow it to take on ordered alignment. This point should be investigated further to examine the potential for material with specific functions derived from both nano- and micro-structuralization. As revealed in earlier research, CNT arrays show promise in the creation of advanced material functionalities (Ding et al., 2007; Velasquez-Garcia et al., 2010).

In any case, if we wish, for instance, to employ the CNT foam as a gas-sensing material, we can control its sensitivity and pattern of response by selecting suitable preparation conditions, which in turn influence the microstructure and nanostructure in the sample. Recently, sensor arrays consisting of different composite materials, a so-called electronic nose, have been fabricated by several researchers (Hu et al., 2004; Lu et al., 2006; Star et al., 2006). Since each conductive composite has its own response characteristics as determined by specific interactions between the polymer matrix and the gas of interest, the response pattern given by the detector array contains hidden information about odour species and concentration, which can be extracted through signal processing. A CNT foam may be an interesting candidate as an electronic nose because it has the potential to provide various responses by changes in its structure. Foam preparations from various CNTs are also of interest in investigations into a wide range of applications. As reported in the literature, CNT foams can be applied, among other things, to bio-scaffolds, electronic parts, and shielding material from electromagnetic radiation (Zawadzak et al., 2009; Gutiérrez et al., 2007a, 2007b; Nakagawa et al., 2011; Thomassin et al., 2008). Further in-depth research into CNT foam should provide tantalizing applications of CNTs.

3.2.2 Application to gas diffusion layers of a fuel cell (PEMFC)

This section describes another attempt at exploring CNT foam applications, which is to apply CNT foams to gas diffusion layers (GDLs) for a proton exchange membrane fuel cell (PEFMC). A PEMFC is constructed from a proton exchange layer, catalytic layers, and GDLs. Pt is usually applied to the catalyst on the proton exchange membrane surface or on the GDLs. The proton exchange layer and the catalytic layers are inserted between the GDLs. The GDL allows uniform access of the fuel gas (e.g. hydrogen) and oxidant (e.g. oxygen) to the catalyst layer (Fig. 14-E).

The performance of PEMFC is determined by properties relating to electrochemical reactions. The particular importance of GDL lies in it being a medium that allows gas diffusion, electron conduction, and the mass-transfer control of water produced during an electrochemical reaction at the catalytic layer. The water transfers through the cathode side of the GDL and is subsequently exhausted from the system or used as a moisture source for the proton exchange membrane. The water flow in the GDL is known as liquid-vapour two-phase flow and is considered to be a critical parameter in fuel cell performance (Chen et al., 2004). The temperature gradient in the GDL is crucial to the water vapour pressure that influences the water mass transfer (Kawase et al., 2008). The thermal conductivity and surface nature are thus important characteristics in the GDL material. Ziegler and Gerteisen (2009) have shown that the surface nature and microstructure of GDLs almost completely determine the liquid water distribution and, as a consequence, affect the power-generating performance of the fuel cell. Therefore, the challenge in preparing potential GDL materials is to satisfy all of these requirements (e.g. good electrical conductivity, low mass-transfer resistance, high thermal conductivity, controlled surface characteristics) with a sensible material design strategy. One possibility may be to employ CNT foams as GDLs.
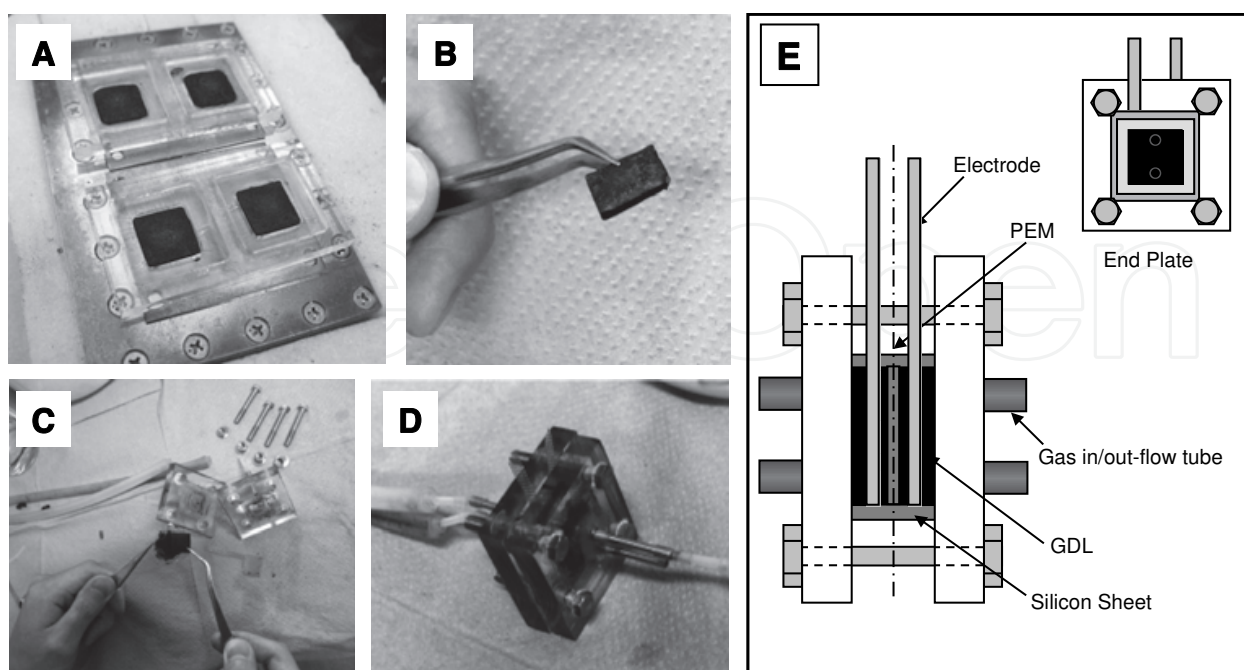

Fig. 14. Setup of PEMFC; (A) CNT foam preparation for PEMFC (contact freezing system), (B) prepared CNT foam, (C, D) assembling a lab-scale PEMFC, (E) assembly instructions.

CNT foams were prepared from an aqueous suspension of CNTs dispersed by chitosan. Thin film-shaped CNT solid foams were prepared (15×15×1 mm), and a lab-scale PEMFC was assembled as shown in Fig. 14. The microstructures of the prepared solid foams can be seen in Fig. 15. As described above, the preparation conditions essentially controlled the microstructures of the prepared CNT foams. The macropores of the prepared carbon foams were heterogeneously distributed in the dried bulk materials, and in general, pores at the top layer were larger than those at the bottom. Increasing the CNT content in the original suspension led to a decrease in mean pore sizes. Furthermore, the amount of CNTs was found to be related to the carbon networks. The carbon foam that contained an excess amount of CNT lost its interconnected carbon networks after preparation. The cooling rate during the freezing step clearly affected the pore sizes. Mean pore sizes decreased with increasing cooling rate.

It was confirmed that the PEMFC assembled with the CNT foams prepared in this study displayed fairly good fuel cell performance. The performance was by no means inferior to that of a fuel cell prepared with conventional carbon paper as GDL material. This suggests that both the CNT content of a freeze-dried bulk and the freezing conditions influenced the performance of prepared fuel cells. It is believed that the carbon networks formed during the freezing step are closely linked to cell performance. Hence, the carbon foam with the defection in its interconnected microstructure did not exhibit good-quality GDL.

Impedance measurement is a useful method of characterizing a battery cell that makes it possible to estimate film resistance and kinetic resistance separately by the adoption of an equivalent circuit model to PEMFC (Fig. 16).
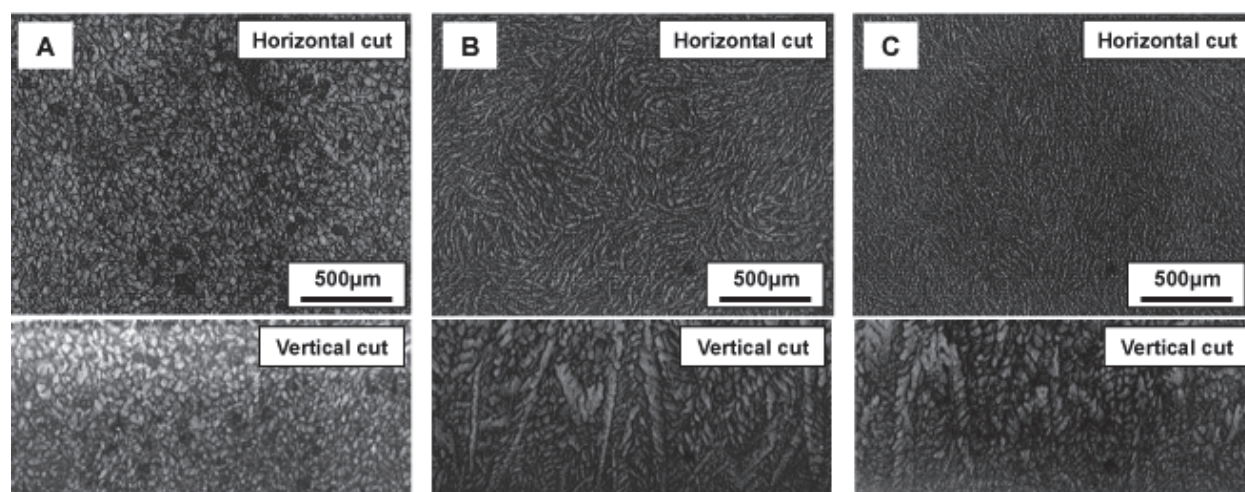

Fig. 15. Microstructures of the prepared CNT foams; (A) Sample-A *(CNT content 15 mg/sheet, prepared via rapid freezing)*, (B) Sample-B *(CNT content 9 mg/sheet, prepared via slow freezing)*, (C) Sample-C *(CNT content 9 mg/sheet, prepared via rapid freezing)*.

It is approximately considered that the film resistance (R_s) corresponds to ohmic resistance such as resistance of the materials and conduction loss at the boundaries of the GDL or membrane. In contrast, the kinetic resistance ($R_s + R_c$) relates to the identical resistance of the device while the circuit is running, which can be regarded as an index of the electrochemical property. The Nyquist diagrams obtained from the impedance measurement on the prepared fuel cells are shown in Fig. 17. We can see that the prepared carbon foams were useful in reducing the film resistances of the PEMFCs, probably owing to the elasticity and
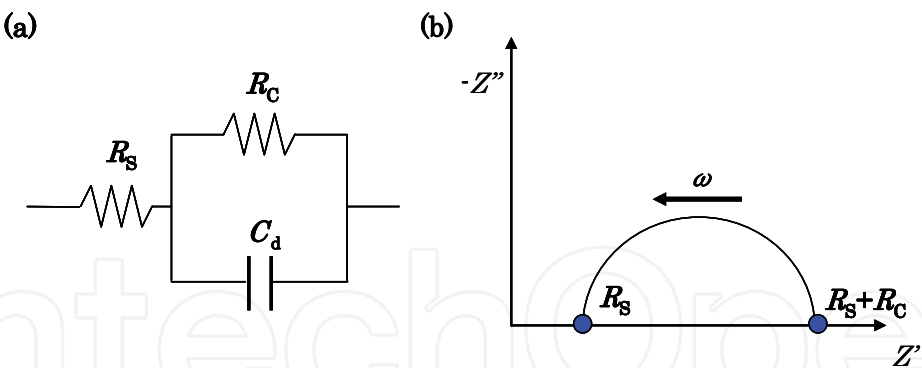
Fig. 16. Equivalent circuit model of PEMFC (a) and Nyquist diagram (b).

specific microstructure of the prepared CNT foams. The kinetic resistances were found to be dependent on the processing conditions of GDLs, that is, the freezing conditions. It is believed that the freezing process controls the degree of overlap among those CNTs that influence the electrochemical properties in a fuel cell. As addressed in the section 3.2.1, it may be that the ice formation controls the nanostructures created by CNT arrays. This idea is further supported by the fact that the thermal conductive characteristics of the prepared solid foams depended on the freezing conditions. Before closing this chapter, it would be interesting to look at the thermal conductivities of the CNT foams that were used in the PEMFC experiment (Table 1). The apparent thermal conductivities of the prepared CNT foams were measured as described in a previous publication (Nakagawa et al., 2011). It was confirmed that the value increased with increasing freezing rate. Although a simple correlation of the values could not be given, it would provide indirect evidence that the nanostructures made by CNT arrays are controlled by ice formation during the freezing step.
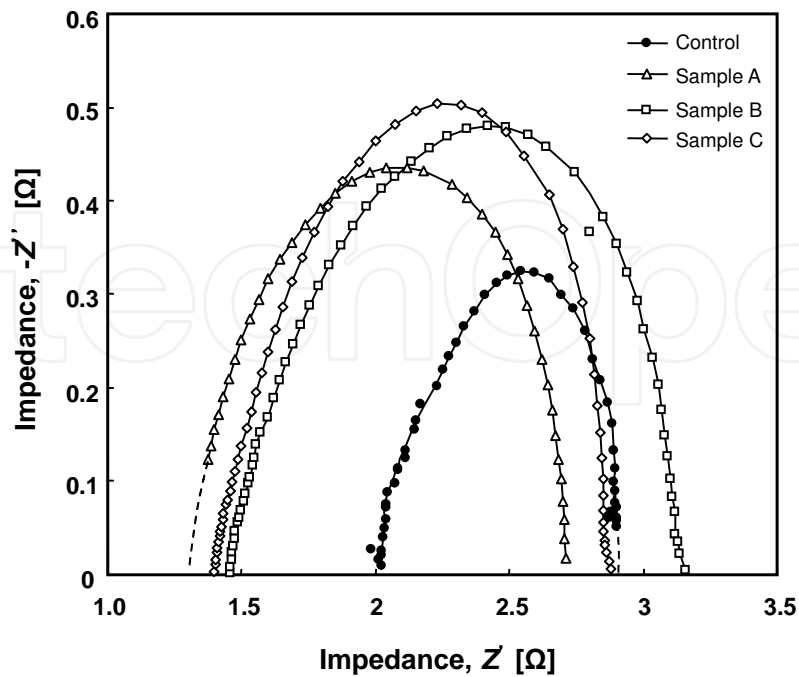

Fig. 17. Nyquist diagrams of the prepared PEMFCs (*samples are as described in Fig. 15: commercial carbon paper was used to obtain control data*).

	Apparent thermal conductivity [W/mK]	Apparent thermal diffusivity [m²/s]
Sample A	0.71	7.4×10^{-6}
Sample B	0.16	2.7×10^{-6}
Sample C	0.42	4.7×10^{-6}
Control (commercial carbon paper)	0.21	0.75×10^{-6}

Table 1. Apparent thermal conductivity of the prepared CNT foams.

4. Concluding remarks

This chapter has described a method of preparing CNT foam preparation using freeze-drying in which the ice formation process could strategically be applied for microstructure control and design. Following solidification theory of a colloidal suspension, ice formation from a CNT aqueous suspension, as expected, created a microstructure in the resultant frozen solution. It was found that the thermal flow during freezing dominated the pattern formation of ice crystals. Therefore, macropores produced in the freeze-dried material (as a replica of ice crystals) may be designed by carefully planning the freezing operation with an external chilling device. Recent literature has shown that unidirectional freezing is key to controlling the microstructure and to creating unique pore structures. However, as pointed out in this chapter, ice microstructure formation cannot be correctly identified without consideration of thermal flow (more specifically, the geometry of the solidification front) in the freezing solution as a whole. From an engineering point of view, sample geometry and thermal flux need to be taken into account in microstructure design. It may be an interesting finding that freezing controls not only the microstructures of freeze-dried CNT foam but also the arrangement of the interconnected CNT arrays (or the degree of overlap). These structural modifications on the nanoscale perhaps determine the subsequent characteristics and functionality of the CNT foams, such as their electronic and thermal properties. It is hoped that the attempts described in this chapter may provide hints for developing applications of CNT foams. The CNT foams demonstrated here remain at the level of prototype and provide scope for future work. For example, it would be interesting to create a composite of an electro-conducting polymer with CNTs for producing a CNT foam (Sweetman et al., 2008).

5. Acknowledgements

6. References

Boccaccini, A.R.; Chicatun, F.; Cho, J.; Bretcanu, O.; Roether, J.A.; Novak, S. & Chen, Q. (2007). Carbon Nanotube Coatings on Bioglass-Based Tissue Engineering Scaffolds. *Advanced Functional Materials*, 17: 2815–2822

Chang, Q.; Zhao, K.; Chen, X.; Li, M. & Liu, J. (2008). Preparation of gold/polyaniline/multiwall carbon nanotube nanocomposites an application in ammonia gas detection. *Journal of Materials Science*, 43: 5861-5866

Chen, J.; Matsuura, T. & Hori, M. (2004). Novel gas diffusion layer with water management function for PEMFC. *Journal of Power Sources*, 131: 155-61.

Chen, L.; Linda, R.O. & Schadler, S. (2010). The influence of carbon nanotube aspect ratio on the foam morphology of MWNT/PMMA nanocomposite foams. *Polymer* 51: 2368-2375

Dash, J.G.; Fu, H. & Wettkaufer, J.S. (1995) The premelting of ice and its environmental consequences. *Reports on Progress in Physics.*, 58: 115–167

Dash, J.G.; Rempel, A.W. & Wettlaufer, J.S. (2006) The physics of premelted ice and its geophysical consequences. *Review of Modern Physics*, 78: 695–741

Deville, S.; Saiz, E. & Tomsia, A. (2007) Ice-templated porous alumina structures. *Acta Materialia*, 55: 1965-1974.

Ding, F.; Lin, Y.; Krasnov, P.O. & Yakobson, B.I. (2007) Nanotube-derived carbon foam for hydrogen sorption. *Journal of Chemical Physics*, 127: 164703

Gutiérrez, M.C.; Garcia-Carvajal, Z.Y.; Hortigüela, M.J.; Yuste, L.; Rojo, F.; Ferrer, M.L. & del Monte, F. (2007a). Biocompatible MWCNT scaffolds for immobilization and proliferation of E. coli. *Journal of Material Chemistry* 17: 2992-2995

Gutiérrez, M.C.; Hortigüela, M.J.; Amarilla, J.M.; Jimenez, R.; Ferrer, M.L. & del Monte, F. (2007b). Macroporous 3D architectures of self-assembled MWCNTs surface decorated with Pt nanoparticles as anodes for direct methanol fuel cell. *Journal of Physical Chemistry C*, 111: 5557–5560

Hermant, M.C.; Verhulst, M.; Kyrylyuk, A.V.; Klumperman, B. & Koning C.E. (2009). The incorporation of single-walled carbon nanotubes into polymerized high internal phase emulsions to create conductive foams with a low percolation threshold. *Composites Science and Technology* 69: 656–662

Hu, J.W.; Chen, S.G.; Zhang, M.Q.; Li, M.W. & Rong, M.Z. (2004). Low carbon black filled polyurethane composite as candidate for wide spectrum gas-sensing element. *Materials Letters*, 58: 3606-3609

Jia, L.; Stevens, M.M.; Zhu, Y.; Gong, Q.; Wu, J. & Lian, J. (2009). Preparation and properties of multi-walled carbon nanotube/carbon/polystyrene composites. *CARBON* 47: 2733–2741

Kawase, M.; Inagaki, T. & Miura, K. (2008). Nonisothermal through-plane transport model of PEMFC with local VLE assumption. *ECS Transaction*, 16: 563-573.

Kwon, S.M.; Kim, H.S. & Jin, H.J. (2009). Multiwalled carbon nanotube cryogels with aligned and non-aligned porous structures, *Polymer* 50: 2786–2792

Lau, C. & Cooney, M.J. (2008). Conductive Macroporous Composite Chitosan-Carbon Nanotube Scaffolds. *Langmuir*, 24: 7004-7010

Leroy, C.M.; Carn, F.; Backov, R.; Trinquecoste, M. & Delhaes, P. (2007). Multiwalled-carbon-nanotube-based carbon foams. *Carbon* 45: 2307–2320

Lu, Y.; Partridge, C.; Meyyappan, M. & Li, J. (2006). A carbon nanotube array for sensitive gas discrimination using principal component analysis. *Journal of Electroanalytical Chemistry*, 593: 105-110

Luis Fernando Velásquez-Garcia, L.F.; Gassend B.L.P. & Akinwande, A.I. (2010) CNT-Based MEMS/NEMS Gas Ionizers for Portable Mass Spectrometry Applications. *Journal of Microelectromechanical Systems*, 19: 484-493

Meng, D.; Ioannou,J. & Boccaccini, A.R. (2009). Bioglass-based scaffolds with carbon nanotube coating for bone tissue engineering. *Journal of Materials Science; Materials in Medicine*, 20: 2139-2144

Nabeta, M. & Sano, M. (2005). Nanotube Foam Prepared by Gelatin Gel as a Template. *Langmuir*, 21: 1706-1708

Nakagawa, K.; Thongprachan, N.; Charinpanitkul, T. & Tanthapanichakoon, W. (2010). Ice Crystal Formation in the Carbon Nanotube Suspension: A Modelling Approach. *Chemical Engineering Science*, 65: 1438-1451

Nakagawa, K.; Yasumura, Y.; Thongprachan, N. & Sano, N. (2011). Freeze-dried Solid Foams Prepared from Carbon Nanotube Aqueous Suspension: Application to gas diffusion layers of a proton exchange membrane fuel cell. *Chemical Engineering and Processing*, 50: 22-30

Nakagawa, K; Hottot, A.; Vessot, S. & Andrieu, J. (2007). Modelling of Freezing Steps during Freeze-Drying of Drugs in Vials. *AIChE Journal*, 53: 1362-1372

Olivas-Armendáriz, I.; Garcia-Casillasa, P.; Martiinez-Sánchez, R.; Martiinez-Villafane, A. & Martínez-Pérez C.A. (2010). Chitosan/MWCNT composites prepared by thermal induced phase separation. *Journal of Alloys and Compounds* 495: 592–595

Park, K.W. & Kim, G.H. (2009). Ethylene Vinyl Acetate Copolymer (EVA)/Multiwalled Carbon Nanotube (MWCNT) Nanocomposite Foams. *Journal of Applied Polymer Science*, 112: 1845–1849

Peppin, S.S.L., Majumdar, A. & Wettlaufer, J.S. (2010) Morphological instability of a non-equilibrium ice-colloid interface. *Proceedings of the Royal Society A*, 466: 177–194.

Peppin, S.S.L., Worster, M.G. & Wettlaufer, J.S. (2007) Morphological instability in freezing colloidal suspensions. *Proceedings of the Royal Society A*, 463, 723–733.

Peppin, S.S.L.; Wettlaufer, J.S. & Worster, M.G. (2008) Experimental Verification of Morphological Instability in Freezing Aqueous Colloidal Suspensions. *Physical Review Letters*, 100: 238301

Quang, N.H.; Trinh, M.V.; Lee, B.H. & Huh, J.S. (2006). Effect of NH_3 gas on the electrical properties of single-walled carbon nanotube bundles. *Sensors and Actuators B*, 113: 341-346

Romanenko, A.I.; Anikeeva, O.B.; Kuznetsov, V.L.; Buryakov, T.I.; Tkachev, E.N. & Usoltseva, A.N. (2007). Influence of helium, hydrogen, oxygen, air and methane on conductivity of multiwalled carbon nanotubes. *Sensors and Actuators A*, 138: 350-354

Sayago, I.; Santos, H.; Horrillo, M.C.; Aleixandre, M.; Fernandez, M.J.; Terrado, E., et al. (2008). Carbon nanotube networks as gas sensors for NO2 detection. *Talanta*, 77: 758-764

Shaffer, S.P.M. & Windle, A.H. (1999). Fabrication and characterization of carbon nanotube/poly(vinyl alcohol) composites. *Advanced Materials*, 11: 937-941

Shen, J.; Zeng, C. & Lee L.J. (2005). Synthesis of polystyrene–carbon nanofibers nanocomposite foams. *Polymer* 46: 5218–5224.

Star, A.; Joshi, V.; Skarupo, S.; Thomas, D. & Gabriel, J.C.P. (2006). Gas sensor array based on metal-decorated carbon nanotubes. *The Journal of Physical Chemistry B*, 110: 21014-21020.

Suehiro, J.; Zhou, G. & Hara, M. (2003). Fabrication of a carbon nanotube-based gas sensor using dielectrophoresis and its application for ammonia detection by impedance spectroscopy. *Journal of Physics D: Applied Physics*, 36: L109-14

Sun, G.; Liu, S.; Hua, K.; Lv, X.; Huang, L. & Wang, Y. (2007). Electrochemical chlorine sensor with multi-walled carbon nanotubes as electrocatalysts. *Electrochemistry Communications*, 9: 2436–2440

Sweetman, L.J.; Moulton, S.E. & Wallace, G.G. (2008). Characterisation of porous freeze dried conducting carbon nanotube-chitosan scaffolds. *Journal of Materials Chemistry*, 18: 5417-5422

Thomassin, J.M.; Pagnoulle, C.; Bednarz, L.; Huynen, I.; Jerome, R. & Detrembleur, C. (2008). Foams of polycaprolactone/MWNT nanocomposites for efficient EMI reduction. *Journal of Materials Chemistry*, 18: 792-796

Thomassin, J.M.; Pagnoulle, C.; Bednarz, L.; Huynen, I.; Jerome, R. & Detrembleur, C. (2008) Foams of polycaprolactone/MWNT nanocomposites for efficient EMI reduction. Journal *of Materials Chemistry*, 18: 792-796

Thongprachan, N.; Nakagawa, K.; Sano, N.; Charinpanitkul, T. & Tanthapanichakoon, W. (2008). Preparation of macroporous solid foam from muti-walled carbon nanotubes by freeze-drying technique. *Materials Chemistry and Physics*, 112: 262-269

Wettlaufer. J.S. & Worster, M.G. (2006). Premelting Dynamics. *Annual Review of Fluid Mechanics*, 38: 427–452

Wilde, G. & Perepezko, J.H. (2000) Experimental study of particle incorporation during dendritic solidification. *Materials Science and Engineering A*, 283: 25–37

Worsley, M.A.; Kucheyev, S.O.; Satcher, J.H.; Hamza, A.V. & Baumann, T.F. (2009). Mechanically robust and electrically conductive carbon nanotube foams. *Applied Physics Letters* 94, 073115

Xiang, Z.; Chen, T.; Li, Z. & Bian, X. (2009). Negative Temperature Coefficient of Resistivity in Lightweight Conductive Carbon Nanotube/ Polymer Composites. *Macromolecular Material and Engineering*, 294: 91–95

Zawadzak, E.; Bil, M.; Ryszkowska, J.; Nazhat, S.N.; Cho, J.; Bretcanu, O.; J.A. & Boccaccini, A.R. (2009). Polyurethane foams electrophoretically coated with carbon nanotubes for tissue engineering scaffolds. *Biomedical Materials* 4: 015008 (9pp)

Zeng, C.; Hossieny, N.; Zhang, C & Wang, B. (2010). Synthesis and processing of PMMA carbon nanotube nanocomposite foams. *Polymer* 51: 655–664

Zhang, S.; Zhang, N.; Huang, C.; Ren, K. & Zhang, Q. (2005). Microstructure and Electromechanical Properties of Carbon Nanotube/ Poly(vinylidene fluoride-trifluoroethylene-chlorofluoro- ethylene) Composites. *Advanced Materials*, 17: 1897-1901

Ziegler, C. & Gerteisen, D. (2009). Validity of two-phase polymer electrolyte membrane fuel cell models with respect to the gas diffusion layer, *Journal of Power Sources*, 188: 184-191

Carbon Nanotubes - From Research to Applications

Edited by Dr. Stefano Bianco

ISBN 978-953-307-500-6

Hard cover, 358 pages

Publisher InTech

Published online 20, July, 2011

Published in print edition July, 2011

Since their discovery in 1991, carbon nanotubes have been considered as one of the most promising materials for a wide range of applications, in virtue of their outstanding properties. During the last two decades, both single-walled and multi-walled CNTs probably represented the hottest research topic concerning materials science, equally from a fundamental and from an applicative point of view. There is a prevailing opinion among the research community that CNTs are now ready for application in everyday world. This book provides an (obviously not exhaustive) overview on some of the amazing possible applications of CNT-based materials in the near future.

How to reference

In order to correctly reference this scholarly work, feel free to copy and paste the following:

Kyuya Nakagawa (2011). Foam Materials Made from Carbon Nanotubes, Carbon Nanotubes - From Research to Applications, Dr. Stefano Bianco (Ed.), ISBN: 978-953-307-500-6, InTech, Available from: http://www.intechopen.com/books/carbon-nanotubes-from-research-to-applications/foam-materials-made-from-carbon-nanotubes

INTECH
open science | open minds